

Violent relaxation of ellipsoidal clouds

David Benhaïem¹ and Francesco Sylos Labini^{2,1,3}

¹*Istituto dei sistemi complessi, Consiglio Nazionale delle Ricerche, Via dei Taurini 19, I-00185 Rome, Italy*

²*Centro Studi e Ricerche Enrico Fermi, Via Panisperna 00184 - Rome - Italy*

³*INFN Unit Rome 1, Dipartimento di Fisica, Università di Roma Sapienza, Piazzale Aldo Moro 2, 00185 Roma, Italy*

18 March 2015

ABSTRACT

An isolated, initially cold and ellipsoidal cloud of self-gravitating particles represents a relatively simple system to study the effects of the deviations from spherical symmetry in the mechanism of violent relaxation. Initial deviations from spherical symmetry are shown to play a dynamical role that is equivalent to that of density fluctuations in the case of an initially spherical cloud. Indeed, these deviations control the amount of particles energy change and thus determine the properties of the final energy distribution, particularly the appearance of two species of particles: bound and free. Ejection of mass and energy from the system together with the formation of a density profile decaying as $\rho(r) \sim r^{-4}$ and a Keplerian radial velocity dispersion profile, are the prominent features similar to those observed after the violent relaxation of spherical clouds. In addition, we find that ejected particles are characterized by highly non-spherical shapes, whose features can be traced in the initial deviations from spherical symmetry that are amplified during the dynamical evolution: particles can indeed form anisotropic configurations, like bars and/or disks, even though the initial cloud was very close to spherical.

Key words: galaxies: formation; galaxies: elliptical and lenticular, cD; methods: numerical

1 INTRODUCTION

The collapse of an isolated, cold and initially spherical cloud of self-gravitating particles has been extensively studied in the literature (Hénon 1973; Van Albada 1982; Aarseth et al. 1988; Bertin 2000; Boily et al. 2002; Joyce et al. 2009b; Sylos Labini 2012, 2013) as it is considered a paradigmatic example of the violent relaxation mechanism. This is the main physical process through which a self-gravitating system reaches a quasi stationary virialized state far from thermodynamic equilibrium. Numerical experiments have shown that the global collapse of the system occurs in a relatively short time scale $\tau_c \sim 1/\sqrt{G\rho_0}$, where ρ_0 is the cloud mass density. For $t \lesssim \tau_c$ the violently changing gravitational field of the system considerably varies individual particle energy (Hénon 1964; Lynden-Bell 1967). This mechanism of energy exchange was called violent relaxation in order to distinguish it from the collisional two-body relaxation which occurs on much longer time scale (Binney & Tremaine 2011).

One of the most peculiar features occurring in the collapse of a spherical and cold cloud is represented by the ejection of a relevant part of its mass (i.e., $\approx 30\%$) and energy. While several authors (see, e.g., Van Albada (1982); David & Theuns (1989); Aguilar & Merritt (1990); Theuns & David (1990); Roy & Perez (2004); Barnes et al. (2009)) noticed this ejection, the importance of this process

with respect to the mechanism of violent relaxation and to the formation of the virialized structure has been overlooked. In a series of works (Joyce et al. 2009b,a; Sylos Labini 2012, 2013) we have shown that the ejection of mass and energy is indeed the crucial mechanism for the formation of the virialized structure density and velocity profiles.

Mass and energy ejection depends on both the initial shape of the density profile and the initial virial ratio (Sylos Labini 2012, 2013). Namely, the largest system contraction occurs for a cold and uniform initial density distribution; if the density profile is described by a power-law function of the distance from the origin, i.e. $\rho(r) \sim r^{-\alpha}$, the collapse gets softer when the exponent gets steeper. Eventually, for $\alpha > 2$ the system does not contract violently anymore and its final configuration does not substantially differ from the initial one (Sylos Labini 2013). On the other hand, when the initial velocity dispersion is large enough, i.e. $b = 2K/W$ with $b < -1/2$ (where K/W is the initial kinetic/potential energy), random motions of the particles oppose to the system gravitational contraction, so that the cloud only slightly changes its initial configuration (Sylos Labini 2012).

Only when particles ejection occurs, the density and the radial velocity dispersion profiles of the remaining virialized structure show the same behavior: in particular it is

observed that the latter scales as $\rho(r) \sim r^{-4}$ while the former scales as $\langle v_r^2 \rangle \sim r^{-1}$. If ejection does not take place then the power-law tails do not form. This tail is indeed made of bound particles with energy close to zero, i.e. with velocity only slightly smaller than the escape one. The universality of the density profile thus originates from the large spread in the energy distribution formed during the violent collapse of the cloud. Because of such large energy change, some of the particles can gain enough kinetic energy to escape from the system while other remain bound to it but with energy very close to zero.

Therefore a spherical and cold cloud represents a very simple initial configuration showing a rich variety of non trivial dynamical behaviors during its evolution. This is however a too idealized situation for an interesting physical initial condition. As a further step towards a more realistic situation we consider in this work the collapse of a cold and isolated ellipsoidal cloud of self-gravitating particles. We show that the initial deviations from spherical symmetry, finely tuned in numerical experiments, can be interpreted to play the same role of density fluctuations for the collapse of a spherical system, determining both the ejection of a fraction of the system mass and the formation of the density and radial velocity profiles decays respectively as $\rho(r) \sim r^{-4}$ and $\langle v_r^2 \rangle \sim r^{-1}$. In addition, we show that both the virialized structure and the ejected particles are characterized by non-spherical shapes, whose characteristics reflect, in a different way, the imprint of the deviations from spherical symmetry characterizing the initial clouds.

The paper is organized as follows: we first describe in Sect.2 the initial conditions we used and the details of the simulations we have performed. Then in Sect.3 we discuss the main features of the violent relaxation mechanism for an initially ellipsoidal cloud. Post-collapse virialized particles shows the same density and radial velocity profiles that are independent of the initial cloud shape: these features, together with the strongly anisotropic configuration of ejected particles, are discussed in Sect.4. Finally we draw our main conclusions in Sect.5.

2 INITIAL CONDITIONS AND SIMULATIONS

We first describe the properties of the initial conditions that we considered for our controlled numerical experiments. Then we discuss the technicalities of the simulations.

2.1 Initial conditions

Initial conditions are represented by an isolated cloud of N particles of equal mass m . The total mass of the system $M = m \cdot N$ is kept constant and thus when the number of particles N is changed their mass scales accordingly, i.e. $m = M/N$. Note that the thermodynamic limit corresponds to

$$\lim_{N \rightarrow \infty; m \rightarrow 0} m \cdot N = M = \text{const.} \quad (1)$$

Particles are distributed randomly with uniform density, i.e. density fluctuations are Poissonian and decay as $\Delta N/N \sim N^{-1/2}$.

Name	ι	τ	ϕ
Sphere	0	—	0
Prolate	x	1	$\approx x/2$
Oblate	x	0	$\approx x/2$
Triaxial	$2x/(2+x)$	1/2	$2x/(4+3x)$
Disk	1	0	1/2
Tiny Cylinder	$\gg 1$	1	≈ 1

Table 1. Oblate ($a_2 = a_3 = a_1 + x > a_1$), prolate ($a_3 = a_2 + x = a_1 + x$) and triaxial ($a_2 = (a_1 + a_3)/2$, where $a_3 = a_1 + x$) ellipsoid: in all cases we take $0 < x \ll 1$.

The cloud has initially an ellipsoidal shape ¹

$$\frac{x^2}{a_1^2} + \frac{y^2}{a_2^2} + \frac{z^2}{a_3^2} = 1. \quad (2)$$

where we take hereafter $a_3 \geq a_2 \geq a_1$. The three eigenvalues of the inertia tensor can be calculated as

$$\lambda_i = \frac{1}{5} M (a_j^2 + a_k^2) \quad (3)$$

where $i \neq j \neq k$ and $i, j, k = 1, \dots, 3$: from the definition of the semi-axes we have $\lambda_1 \geq \lambda_2 \geq \lambda_3$ — note that λ_1 is oriented in the direction of the smallest semi-axis a_1 and λ_3 in the direction of the largest one a_3 .

To characterize the structure shape we define three different linear combinations of λ_i : the flatness parameter²

$$\iota = \frac{\lambda_1}{\lambda_3} - 1, \quad (4)$$

the triaxiality index

$$\tau = \frac{\lambda_2 - \lambda_3}{\lambda_1 - \lambda_3} \quad (5)$$

and the disk parameter

$$\phi = \frac{\lambda_1 - \lambda_3}{\lambda_2 + \lambda_3}. \quad (6)$$

Note that the combination of ι, τ and ϕ allows one to distinguish not only between different type of ellipsoids (prolate, oblate and triaxial) but also between other shapes like bars and disks. In Tab.1 we report their values for some paradigmatic cases.

2.2 Simulations

We have performed $N_r = 10$ different simulations of the same cloud but with different realizations of the initial Poisson noise. We have computed averages of the various physical quantities over the different realizations of the cloud. In

¹ Our units are such that, for the spherical case $a_1 = a_2 = a_3 = R_c$ we have $\rho_0 = M/(4\pi R_c^3/3) = 1 \text{ gr/cm}^3$ so that the characteristic time scale for the collapse (see Eq.8) is $\tau_c = 2100$ seconds

² Note that these parameters are generally defined in function of the semi-axis a_1, a_2, a_3 and not in function of the eigenvalues (see Eq.3). However for small deformations of a perfect sphere (those that we considered here) these definitions are almost equivalent. The advantage of using the eigenvalues to define these parameters is that this choice allows one to describe more easily shapes that differ from ellipsoids.

addition, we considered two set of clouds with $N = 10^4$ and $N = 10^5$ particles and same total mass.

We have used the parallel version of the publicly available tree-code **Gadget** (Springel et al. 2001; Springel 2005) to run N-body simulations. We used a softening length ε , i.e. the scale below which the two-body potential is not Newtonian anymore, such that $\varepsilon/\ell(t=0) \ll 1$, where $\ell(t=0)$ is the initial inter-particle distance. In order to choose a proper value for ε that does not affect the gravitational dynamics during the *whole* time range of the simulations (i.e. $t < 10\tau_c$), we have considered a necessary (but a priori not sufficient) condition: ε must be smaller than the system size at all times. As typical radius of the system we took the gravitational one:

$$R_g(t) = \frac{GM_b(t)}{|W_b(t)|} \quad (7)$$

where $M_b(t)$ and $W_b(t)$ are respectively the mass of the bound system and its potential energy at time t . We numerically determine the minimal value R_g^{min} of $R_g(t)$ during the time evolution, that occurs for times close to the collapse time τ_c ; we thus require that $R_g^{min} \gg \varepsilon$. Clearly at $t \approx \tau_c$ the inter-particle distance is $\ell(\tau_c) \ll \varepsilon$, so that two-body scatterings can highly differ from a pure Newtonian situation. However the typical time scale of two-body scatterings is far longer than the typical collapse time scale: for this reason collisional effects should not be dominant during the collapse phase.

In order to test the effects of collisionality we have performed several tests by varying the smoothing length ε in **Gadget** (and the appropriate time-step parameters) and we have carefully followed the collapse. Our conclusion, that agrees with that of Joyce et al. (2009b), who considered the collapse of a initially cold, spherical and uniform cloud (for which the collapse is stronger), is that as long as we have $\varepsilon < R_{min}$, collisionality does not play an important role in the violent collapse phase of these systems.

In addition, we found that the necessary condition $\varepsilon \ll R_g^{min}$ is also a sufficient one, as not only the numerical integration conserves total energy and momentum up to a few percent but also macroscopic quantities describing the system we are interested in, as the density and velocity profiles, the global shape, etc., do not show a detectable dependence on ε . In particular, we have found a good convergence of the results for $R_g^{min}/\varepsilon \in [10, 200]$. On the other hand when $\varepsilon \geq R_g^{min}$ the gravitational dynamics is modified at the scale of the system and one detects large deviations with respect to the $\varepsilon < R_g^{min}$ case (see also discussion in Joyce et al. (2009b); Sylos Labini (2012)).

Beyond the softening length, the precision of a **Gadget** simulation is determined by the internal time-step accuracy η and by the cell-opening accuracy parameter of the force calculation α_F . We have chosen the time-step criterion 0 of **Gadget** with $\eta = 0.025$. In the force calculation we employed the (new) **Gadget** cell opening criterion with a force accuracy of $\alpha_F = 0.001$ (Springel et al. 2001; Springel 2005).

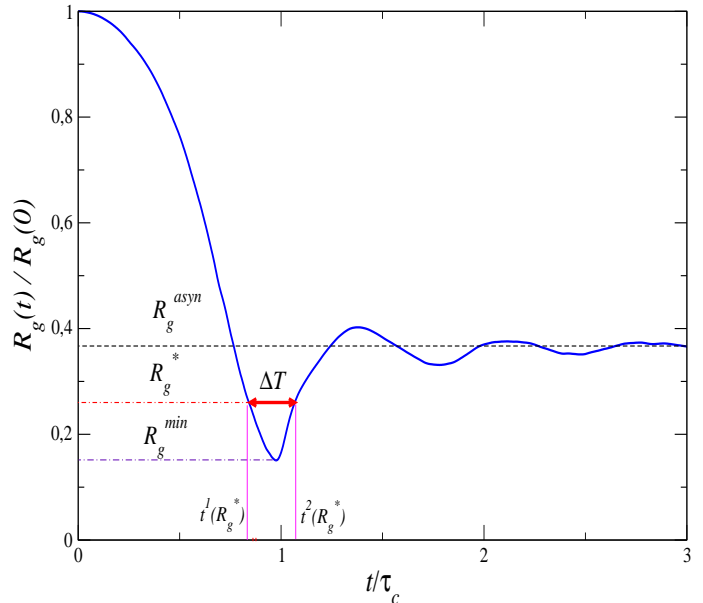


Figure 1. Example of the behavior of the gravitational radius (scaled to its initial value $R_g(0)$) as a function of time when the initial condition is a cold spherical cloud. It is also shown the method we choose to estimate the duration of the collapse.

3 VIOLENT RELAXATION MECHANISM FOR AN ELLIPSOIDAL CLOUD

We first review in Sect.3.1 the main elements of the violent relaxation mechanism for initially spherical clouds with different discretization but same total mass. Then in Sect.3.2 we discuss the case of an initially ellipsoidal cloud considering how to map one problem into the other.

3.1 The spherical case

For an idealized initial spherical cloud all particles have the same collapse time, i.e. they arrive at the center simultaneously:

$$\tau_c \equiv \sqrt{\frac{3\pi}{32G\rho_0}}, \quad (8)$$

where $\rho_0 = 3M/(4\pi R_c^3)$. In the thermodynamic limit (i.e., when fluctuations can be neglected) the collapse can be described as the simple gravitational contraction of a perfectly homogeneous cloud. This simple idealization well describes the observed collapse for $t < \tau_c$. Because of the effect of density fluctuations, the same approximation fails to follow the system behavior for $t \geq \tau_c$ (Joyce et al. 2009b), i.e. when the system size should nominally reduce to zero to then re-expand in a periodic way. Instead, for $t > \tau_c$ a simulated cloud relaxes into a quasi stationary state with its size remaining almost constant (see Fig.1).

Several authors (see, e.g., Aarseth et al. (1988); Boily et al. (2002); Joyce et al. (2009b) and references therein) found that the minimal gravitational radius of the

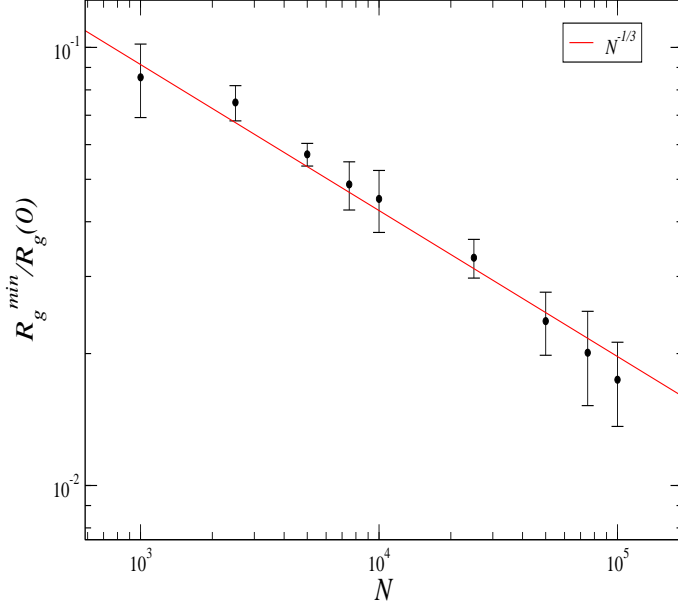


Figure 2. Gravitational radius (see Eq.9) for an initial spherical cloud with different values of N .

bound structure R_g^{min} scales as

$$R_g^{min} \sim N^{-1/3}. \quad (9)$$

This relation physically means that the system stops collapsing, reaching its minimal size, when N density fluctuations on the scale of the systems itself go nonlinear: Eq.9 nicely fits the observed behavior as shown in Fig.2.

When N is finite, the free fall time spread is related to the initial density fluctuations. From Eq.8 we simply get

$$\frac{\Delta T}{\tau_c} \sim \frac{\Delta \rho}{\rho_0} \sim N^{-1/2}, \quad (10)$$

which approximates well the data (see Fig.3). Note that in the simulations ΔT has been estimated as the width of $R_g(t)$ around its minimum³.

During the collapse a fraction of the particles may gain enough kinetic energy to escape from the system. In particular the fraction of ejected particles shows a slow log-dependence with N (see Fig.4) in agreement with the results of Joyce et al. (2009b). We recall that there was no theoretical explanation for this behavior and we will come back on this point in Sect.3.2. The mechanism of particles energy gain originates from the coupling of the growth of density fluctuations with the system finite size. Particles originally placed close to the system boundaries develop a net lag with respect to the bulk, thus arriving at the system center when the others are already re-expanding. These particles, by moving in a rapidly varying gravitational field

³ To estimate ΔT we define the two values of the gravitational radius for $t < \tau_c$ and $t > \tau_c$ such that $R_g^* = R_g^{min} + (R_g^{asy} - R_g^{min})/2$ where R_g^{asy} is gravitational radius reached for $t > \tau_c$. Then the duration of the collapse is defined as $\Delta T = t^2(R_g^*) - t^1(R_g^*)$ (see Fig.1).

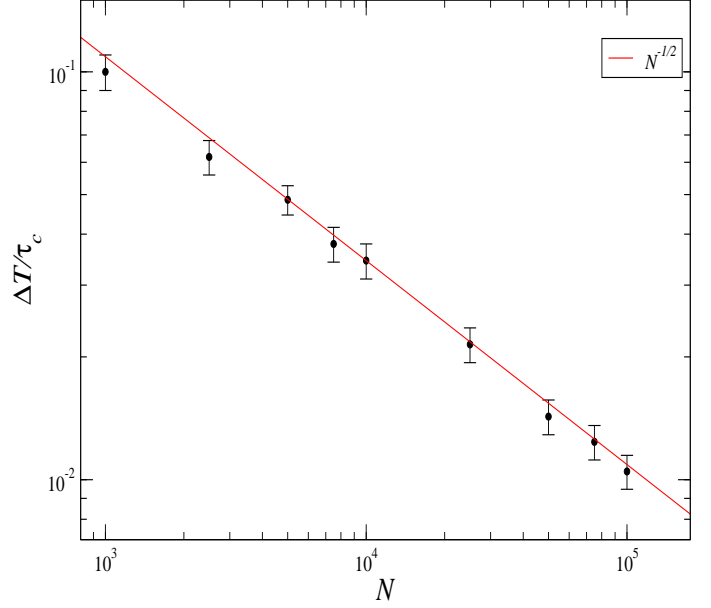


Figure 3. Behavior of the spread of free fall times ΔT (normalized to τ_c) for an initial spherical cloud and different values of N .

can gain kinetic energy and can drastically change the whole energy distribution (Joyce et al. 2009b).

The energy change particles undergo when passing through the center has also an angular dependence that reflects the initial deviation from perfect spherical symmetry. Indeed, the flatness parameter (Eq.4) is initially different from zero because of Poisson fluctuations

$$\iota(0) \approx \frac{1}{\sqrt{N}}. \quad (11)$$

This initial small deviation from perfect spherical symmetry is amplified during the collapse phase because of the large particles energy change. Eq.11 implies that the system is not initially perfectly spherical, but it can be described as an ellipsoid with $\lambda_1 > \lambda_3$ (i.e. $a_1 < a_3$). According to the energy gain mechanism we described above, particles arriving later at the center, i.e. those initially placed in the range $a_2 < r < a_3$, get the largest energy kick. Some of them are ejected but others are still bounded for $t > \tau_c$. A simple ansatz to describe the deformation was introduced by Worrakitpoonpon (2015); Sylos Labini, Benhaïem & Joyce (2014): if ΔT is the time during which energy is exchanged, we can estimate that the difference between the major and minor semi-axis is

$$\iota(t > \tau_c) \sim \Delta T \cdot \Delta v_c, \quad (12)$$

where v_c is the typical particle velocity at the collapse time. This simply means that difference in the linear dimension between a_3 and $a_1 < a_3$ of the structure depends on the time interval ΔT characterizing the collapse and on the difference in velocity Δv_c between particles in different directions, e.g. along the largest and the smallest semi-axis. Given that the structure is close to virial equilibrium around $t \approx \tau_c$ we have

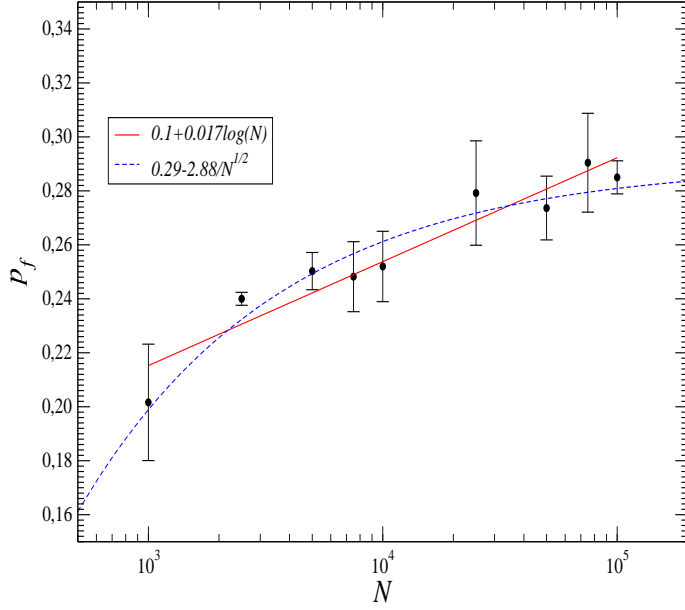


Figure 4. Fraction of ejected particles for different values of N . The best fit $p_f = 0.1 + 0.017 \log(N)$ is a “blind” numerical result, while the fit $p_f = 0.29 - 2.88/\sqrt{N}$ will be discussed in Sect.3.2.

$2K_b \approx |W_b|$ and

$$\Delta v_c \approx v_c \approx \sqrt{|W_b|} \sim \sqrt{\frac{1}{R_g^{min}}}. \quad (13)$$

We thus get

$$\iota(t > \tau_c) \sim \frac{1}{N^{1/2}} \cdot N^{1/6} \sim N^{-1/3} \quad (14)$$

where we used Eq.10, Eq.9 and Eq.13.

We have estimated ι for the 80 % more bounded particles (i.e., $\iota_{80\%}$ — this choice avoids the signal to be affected by large fluctuations), at $t_{max} = 5\tau_c$ and we considered averages over the different realizations. As shown in Fig.5 (where, for comparison, we report the behavior of the initial flattening ratio $\iota_{80\%}(0)$) the agreement between Eq.14 and the data is very good over two orders of magnitude in N .

According to the mechanism of energy gain we have discussed above, we expect: the largest semi-axis of (i) the initial cloud at $t = 0$ (ii) the bound particles at t_{max} and (iii) the free particles at t_{max} should be parallel. We call ψ the angle between (i) and (iii) and φ the angle between (ii) and (iii)⁴. The results are shown in Fig.6: the probability density function for both ψ and φ are peaked at 0 showing that these axes are parallel among each other. In particular, ejection occurs more likely in the direction of the the initial largest semi-axis, while the final virialized structure is less correlated with such a direction.

⁴ these are measured from the computation of the corresponding eigenvalue $\tilde{\lambda}_3$ for bound a free particles at $t =, t_{max}$.

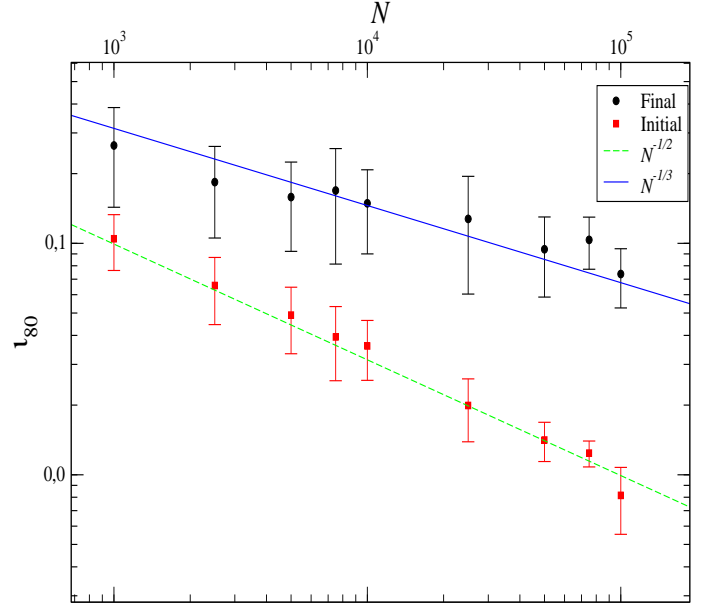


Figure 5. Behavior of $\iota_{80}(5\tau_c)$ and of the initial flattening ratio $\iota_{80}(0)$ (i.e., Eq.11) as a function of N

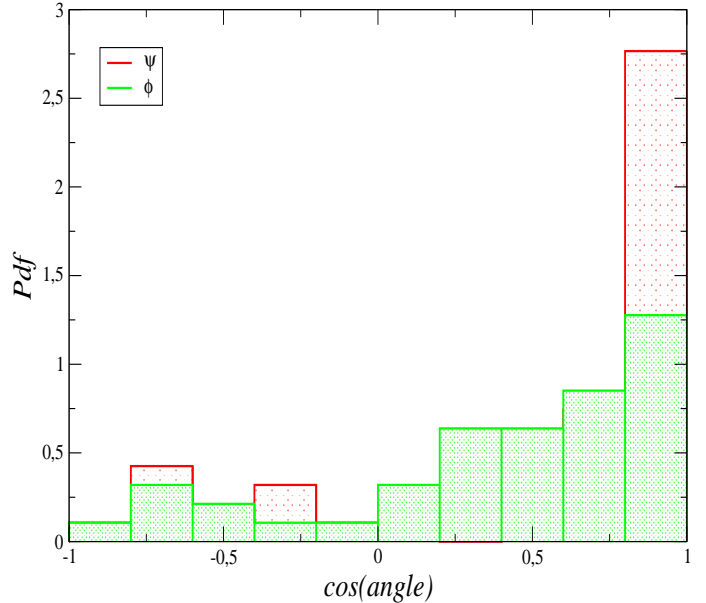


Figure 6. Probability density function (PDF) for the angles ψ and φ (see text).

3.2 The ellipsoidal case

When the initial cloud shape is a prolate ellipsoid then its initial asymmetry is amplified by the violent relaxation mechanism in a way that is equivalent to that of a spherical cloud. However, in this situation the amplitude of the deviation from spherical symmetry, instead of being controlled

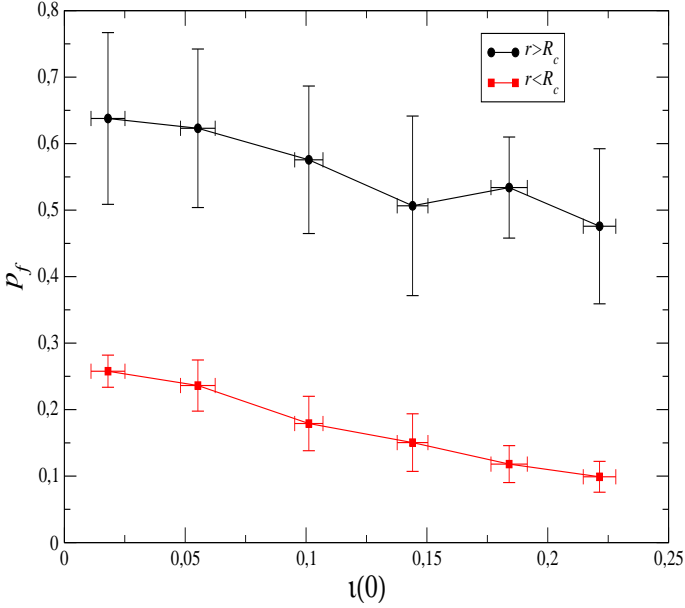


Figure 7. Black (red) dots show the fraction of particles initially with $r > R_c$ ($r < R_c$) that are ejected after the collapse (average over 20 realizations).

by Poisson fluctuations (i.e., Eq.11) is tuned by the ratio between the largest a_3 and the smallest $a_2 = a_1$ semi-axis⁵.

Indeed, we find that, as for spherical case, ejected particles are mostly those which originally lie close to the boundaries of the system: i.e. particles for which initially $r_0 > R_c = a_1$ (see Fig.7). In addition, Fig.8 shows the histogram of the values of ψ, φ (see Sect.3.1 for definitions) for three different sets of simulations with different initial $\iota(0)$. The result is similar to the spherical case (see Fig.6): the largest semi-axis of the initial conditions and of the post collapse bound and free particles are parallel among each other.

According to the model of ejection and system deformation discussed for the spherical case, the increase of $\iota(0)$ corresponds to a decrease in the number of particles for an initially spherical cloud (see Eq.11) so that: (i) the spread in arrival time ΔT increases and the collapse becomes softer as particles arrive at the center at different times, (ii) the fraction of ejected particles decreases and (iii) the minimum gravitational radius reached during time evolution becomes larger:

- Fig.9 shows that the spread in the arrival time ΔT increases linearly with $\iota_{80}(0)$. This can be easily explained by considering that the spread of arrival time ΔT is equal to the difference between the free fall time respectively of a particle initially placed at $R_c(1 + \iota(0))$ and of a particle initially placed at R_c (for small enough $\iota(0)$):

$$\Delta T \approx \sqrt{\frac{3\pi^2}{8G\rho_0}} \left(\sqrt{(1 + \iota(0))^3} - 1 \right) \approx \frac{3}{2} \tau_c \iota(0). \quad (15)$$

⁵ We consider a situation in which the initial flatness ratio is larger than Poisson fluctuations, i.e. $\iota(0) \gg N^{-1/2}$

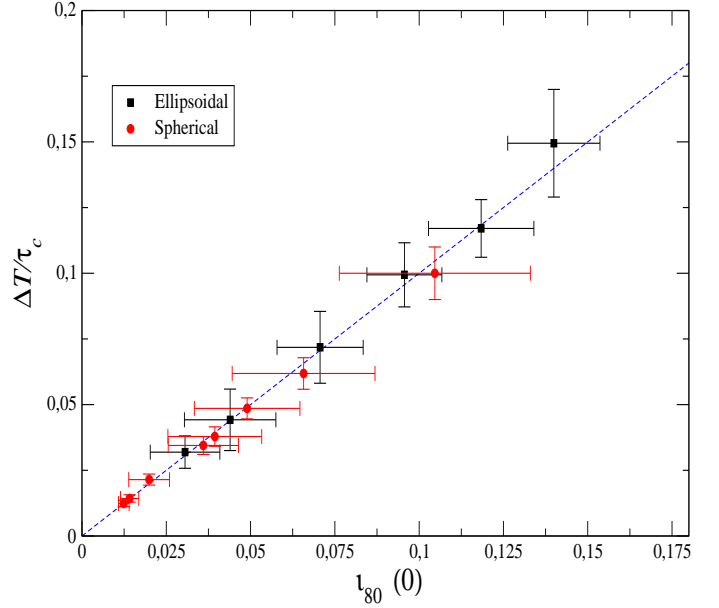


Figure 9. Average over 20 realizations of the spread in the arrival time ΔT versus the initial flattening ratio $\iota(0)$ for the case of ellipsoidal initial conditions (black dots). In addition we plot ΔT versus the actual initial flattening ratio for the simulations of a purely spherical cloud with different N (red dots), i.e. $\iota(0) \sim N^{-1/2}$ — see Fig.5.

(For the spherical cloud we used Eq.10 and Eq.11 to compute ΔT in function of $\iota(0)$.)

- Fig.10 shows the fraction of ejected particles as a function of $\iota_{80}(0)$ for both the ellipsoidal and the spherical clouds: p_f decreases with $\iota(0)$ as the collapse gets softer. In particular, we note that $p_f \propto \iota(0)$ for both the ellipsoidal case at fixed N and varying $\iota(0) > N^{-1/2}$ and for the spherical case with varying N and thus with $\iota(0) \sim N^{-1/2}$. This result suggests a straightforward interpretation of the fraction of mass ejected in function of the number of particles N for the spherical case (see Fig.4) in terms of finite-size N -dependent deformation of the initial spherical cloud. In addition, if we extrapolate the behavior for $\iota(0) \rightarrow 0$, which for the spherical case corresponds to $N \rightarrow \infty$, we find that there is a saturation in the fraction of mass ejected⁶.

- Fig.11 reports the minimum value of the gravitational radius during time evolution R_{min}^g as a function of $\iota(0)$ for both spherical and ellipsoidal initial conditions, with different N and $\iota(0)$ respectively, together with the theoretical fit:

$$R_{min}^g \sim \iota(0)^{2/3} \quad (16)$$

where we used, for the spherical case, Eq. 9 and Eq.11. Again the agreement is extremely good showing that the collapse depth is controlled by $\iota(0)$, which plays, for small enough values, the same role of density fluctuations.

The asymptotic value of $\iota_{80\%}$ as a function of $\Delta T \times$

⁶ For a discussion about the Vlasov-Poisson limit of this system see Joyce et al. (2009b)

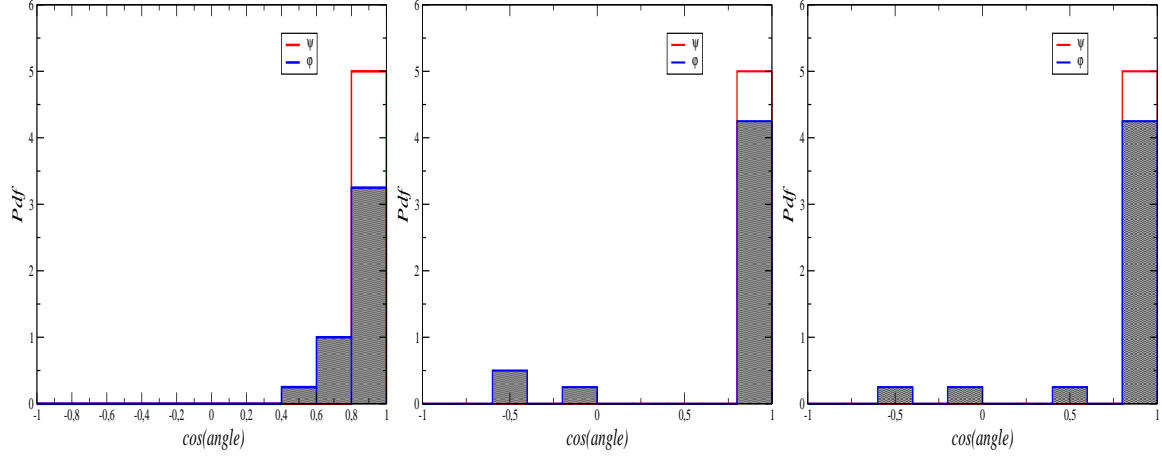


Figure 8. As Fig.6 but for simulations with initial flattening ratio $\iota(0) = 0.05, 0.15, 0.25$ (from left to right).

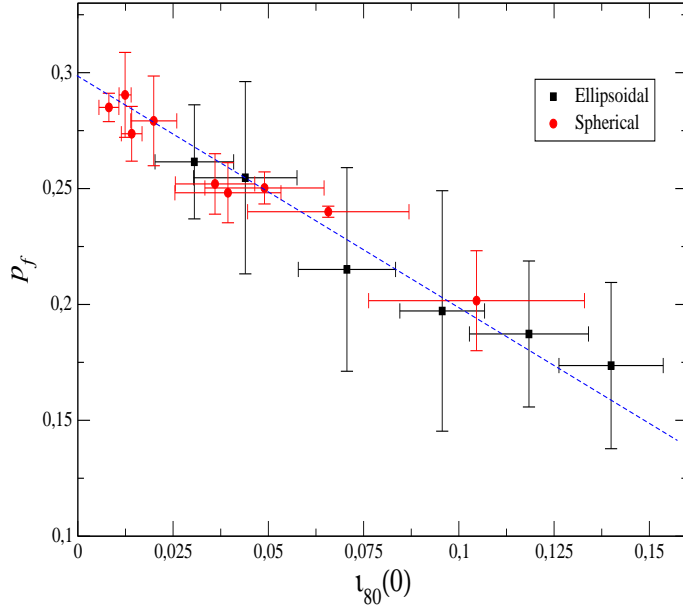


Figure 10. Average over 20 realizations of the fraction of ejected particles vs $\iota_{80}(0)$ (black dots). The case of a uniform sphere with different N is also shown (red dots). The dashed line corresponds to the fit $p_f \sim 1/\sqrt{N} + \text{const.}$ in Fig.4.

R_g^{\min} , for different initial flattening ratios and averaged over 20 realizations, is shown in Fig. 12. We note that the linear behavior described by Eq.12 nicely fit the observed behavior for the spherical simulations. However for the ellipsoidal case, when $\iota(0) > 0.1$, the asymptotic value of ι_{80} clearly deviates from the simple growing behavior. This occurs because of the formation of substructures, a situation that clearly becomes more complex than the one we considered above.

In summary the violent relaxation mechanism as illustrated by Figs.9-11 applies equally well to both the spherical

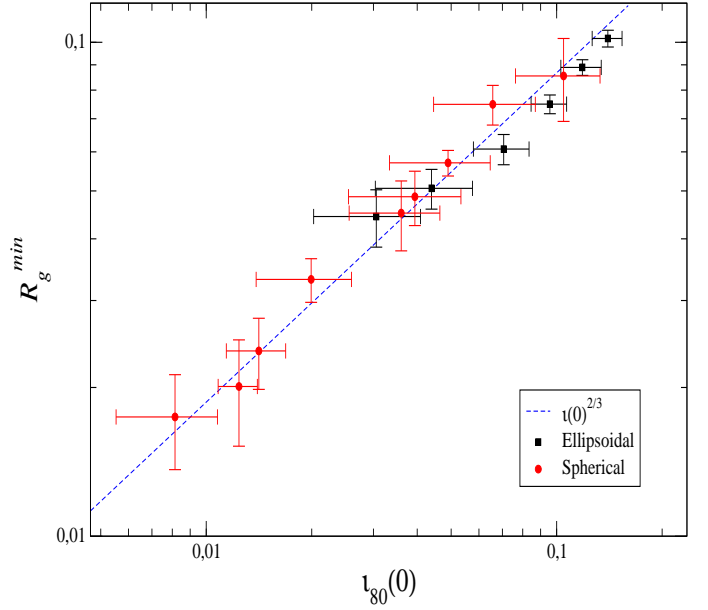


Figure 11. Average over 20 realizations of the minimum of the gravitational radius vs $\iota(0)$ (black dots). The case of a uniform sphere with different N is also shown (red dots). The dashed line represents the fit with Eq.16.

and the ellipsoidal initial conditions, considering that finite N density fluctuations in the former case play the same role of the ratio between the largest and the smallest semi-axis in the latter case.

4 VIRIALIZED AND EJECTED PARTICLES

We first discuss the properties of the virialized structure formed after the gravitational collapse, highlighting that some of their main statistical properties, such as the density

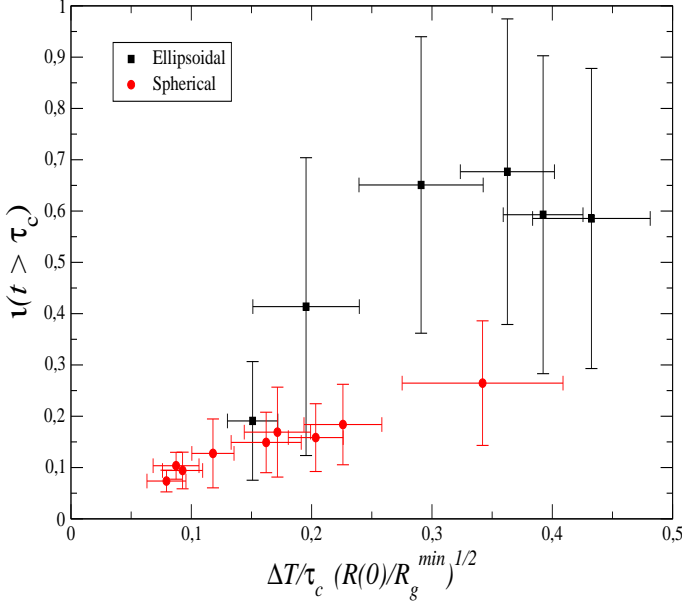


Figure 12. Evolution of the asymptotic value of ι as a function of $\Delta T \times \sqrt{R_g^{min}}^{-1}$, for both ellipsoidal and spherical initial conditions. Eq.(12)

and velocities profiles, are formed during the violent relaxation mechanism and do not show an imprint of the initial conditions. This result, of course, does not hold in general for any cold initial density profile: the identification of the phase space parameters of a cold initial cloud for which the same density and velocity profiles are formed goes beyond the scope of the present work. Then, we describe the different configurations that ejected particles can form, which instead depend on the initial cloud shape.

4.1 The universal density and velocity profiles of bound particles

As mentioned in the introduction, it was recently shown that the post-collapse virialized structure, formed when a cloud is initially cold enough, has a universal density profile. That is, the same profile was found when the initial density profile was uniform, power law with $0 \leq \alpha \leq 2$, Plummer, Gaussian or Hernquist (Sylos Labini 2013). The best fit density profile is

$$\rho(r) = \frac{\rho_0}{1 + (r/r_0)^4} \quad (17)$$

where, in the uniform case, ρ_0 and r_0 depend on the number of points N . This profile was shown to form when bound particles can have energies close to zero, so that they are allowed to orbit mostly in radial trajectories around the dense core, forming thus the $\rho(r) \sim r^{-4}$ tail (see Fig.13). We stress that this situation occurs when a fraction of the system particles get positive energy after the collapse. Thus the mass and energy ejection and the formation the $\rho(r) \sim r^{-4}$ profile are two aspects of the same phenomenon intrinsic to the violent relaxation mechanism.

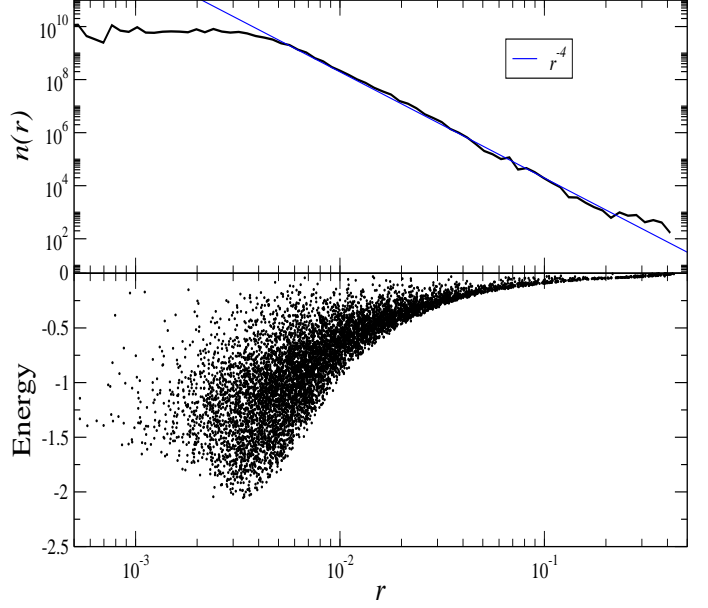


Figure 13. Upper panel: Density profile for the virialized state formed in the collapse of a spherical cloud (a line with slope r^{-4} is plotted for reference). Bottom panel: particle energy (for bound particles only and in normalized units) as a function of the distance from the center of mass.

Fig.14 shows that Eq.17 gives an excellent fit also when the initial condition is an ellipsoid; this fact suggests a common origin for the density profile as an outcome of the violent relaxation mechanism. In addition, the radial velocity dispersion shows a Keplerian behavior for all cases (see Fig.16) which is a further key element in the physical model for the formation of the $\sim r^{-4}$ tail. This means that the initially ellipsoidal cloud, in the range of parameter space considered here, shows the same gravitational collapse dynamics as the spherical clouds. In particular, the virialized structure emerging from the violent relaxation share the same density and velocity profiles. As argued in Sylos Labini (2012, 2013) these are formed during the violent relaxation mechanism because of the large energy changes which particles undergo during the collapse.

As noticed above, the remnants of cold collapses of initially ellipsoidal clouds are strongly non-spherical. In order to take into account the elongated cloud shape, ellipsoidal shells of particles are used in the density profile calculation: in particular, we computed the density profile in ellipsoidal shells with parameters proportional to (and smaller of) those of the final structure. In Fig.15 we show density profiles and their respective fits, using elliptical and spherical shells for the case $\iota(0) = 0.15$. While the free parameters ρ_0 and r_0 are different for these two profiles, one can see that Eq.17 still provides an excellent fit to the density profile.

The distinctive feature of the violent relaxation mechanism is represented by the large particle energy change. This is illustrated in Fig.14 (lower panel), where it is plotted the initial and final particle energy distribution $P(e)$ for $\iota(0) = 0.05$ and $\iota(0) = 0.25$. As the collapse is softer in the former case, the final $P(e)$ has a smaller spread than for case

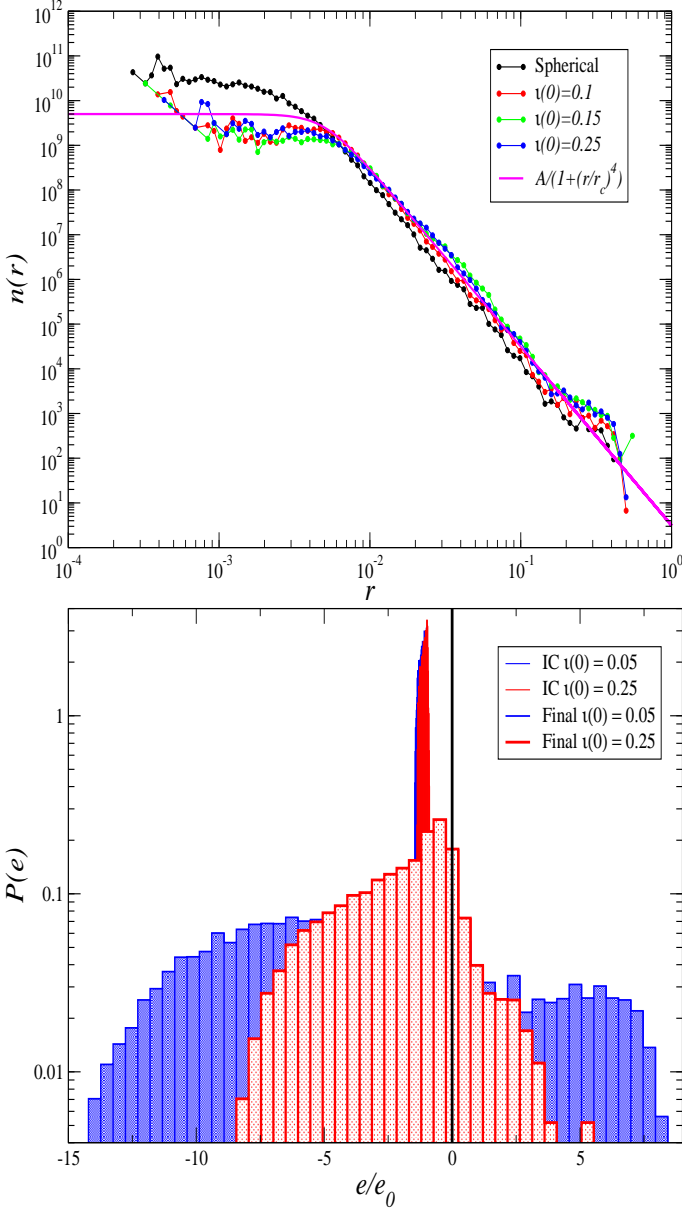


Figure 14. Upper Panel: Density profile for clouds with different initial shape: spherical and prolate ellipsoidal with $\iota(0)$ as reported in the labels. As a reference we have also reported the behavior of the quasi equilibrium profile. Lower panel: particle distribution energy at both the initial and the final time for ellipsoidal initial conditions respectively with $\iota(0) = 0.05$ and $\iota(0) = 0.25$. The particle energy e has been normalized to e_0 , the absolute value of the the potential energy of a particle placed at distance R_c from the center of a uniform spherical cloud.

$\iota(0) = 0.05$: in particular, both the small and high energy tails are reduced. This corresponds to the fact that the final core is less dense and there are fewer ejected particles.

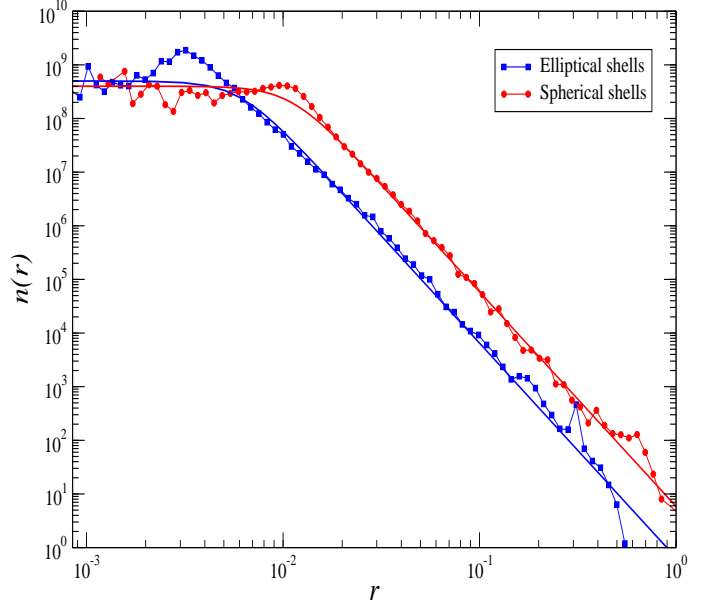


Figure 15. Profiles calculated with ellipsoidal shells and spherical shells, for the case $\iota(0) = 0.15$.

4.2 The asymmetric feature of particle ejection

As discussed above, because ejected particles are those initially at $a_1 = a_2 \leq r \leq a_3$, they are not spherically symmetric neither initially nor for $t > \tau_c$: indeed, the collapse amplifies their initial asymmetry resulting in a very anisotropic final distribution. To characterize their shapes we measure the ι, τ and ϕ (see the upper panel of Fig.17): we may see that by increasing $\iota(0)$, ejected particles do not maintain spherical symmetry (as for $\iota(0) = 0$). Instead, they first tend to form a flat structure and then a bar for $\iota(0) > 0.1$ (see Fig.17). Obviously particles ejected on the two opposite sides of the virialized structure will have velocities oriented in opposite directions, i.e. they will be anti-correlated. When the initial ellipsoid is oblate then ejected particles form a triaxial structure. Indeed, Fig.18 (upper panel) shows that $\iota \approx 2\phi$ and $\tau \approx 1/2$. Finally for a triaxial initial cloud ejected particles form an anisotropic structure that clearly depends on the choice of the initial axes (see Fig.19).

As we can see in Figs. 17, 19 and 18 by changing the value of the initial flatness ratio $\iota(0)$ and the initial shape of the structure (i.e. prolate, oblate or triaxial) one can form different final distributions of ejected particles which are close to flat. While in most cases the majority of the free particles are ejected within a bar along the major semi-axis of the final structure, we note that for the oblate case, especially when $\iota(0) = 0.05, 0.1$, the distribution of the ejected particles is closer to that of a disk.

5 DISCUSSION AND CONCLUSIONS

The gravitational collapse of an initially cold and ellipsoidal cloud of particles shows non-trivial characteristics: some of them are similar to the ones observed when an initially

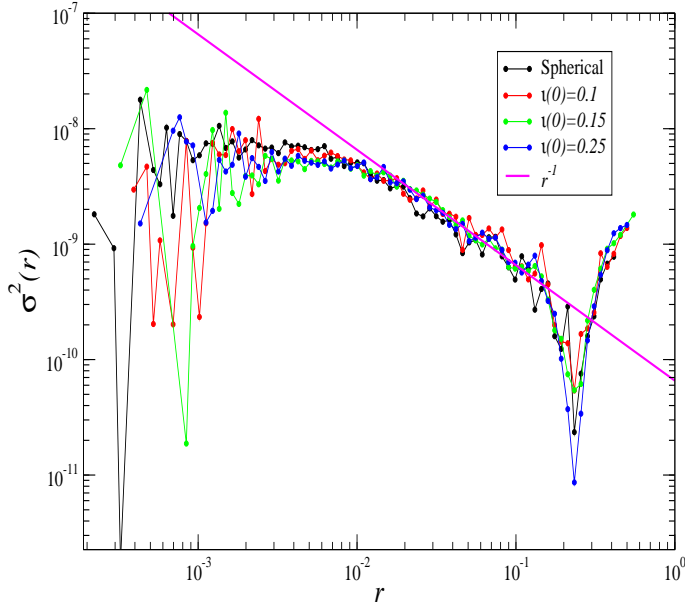


Figure 16. Radial velocity dispersion for clouds with different initial shape. As a reference we have reported also the Keplerian $1/r$ behavior.

spherical cloud is considered as an initial condition. In particular, we have focused our attention on the the formation of power-law density and radial velocity profiles and on the ejection of a fraction of mass and energy from the system. The analogy between the spherical and the ellipsoidal cloud collapse can be understood considering that the initial deviations from spherical symmetry in the former case plays the same dynamical role of density fluctuations in the latter one.

Indeed, we have shown that in the ellipsoidal case the ratio between the largest a_3 and smallest a_1 semi-axis play the same role of density fluctuations for a spherical cloud. Indeed, N randomly placed particles in a sphere, have an intrinsic ellipsoidal deformation $\propto \sqrt{N}^{-1}$ due to Poisson fluctuations; thus increasing N has the same effect of decreasing the difference between a_3 and a_1 . We have discussed in detail that the mechanism of particles energy gain during the collapse gives rise to the ejection of those particles that are initially placed close to the cloud boundaries: for an ellipsoidal cloud this implies an asymmetric ejection.

Thus, the virialized state formed after the collapse of an ellipsoidal cloud shows the same features of the cold spherical cloud remnant: in both cases the density and radial velocity profiles arise from the violent relaxation mechanism. Spherical clouds with different density profiles can however form different virialized structures and a more complete study of the cloud parameters phase space is necessary to draw more general conclusions about quasi-equilibrium profiles.

Note that the mechanism described here is, in principle, different from the the radial orbit instability discussed by Antonov (1961); Fridman & Polyachenko (1984). This instability characterizes a different case from the one considered

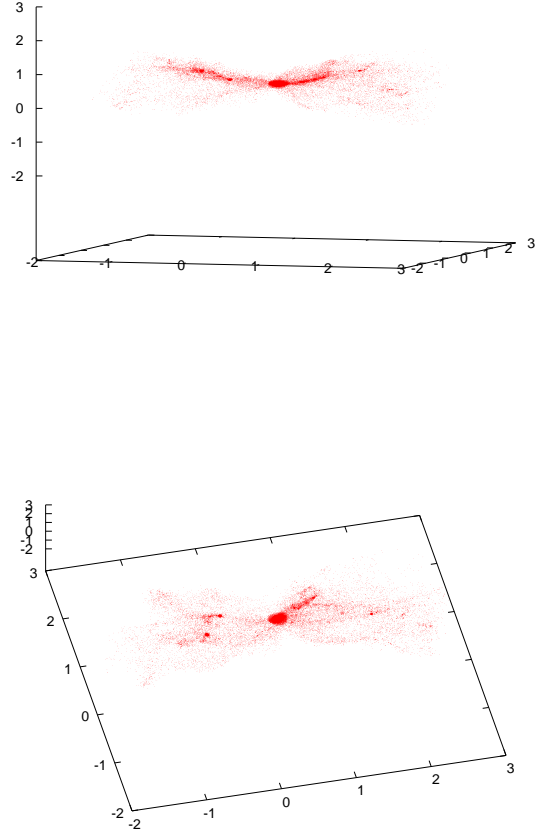
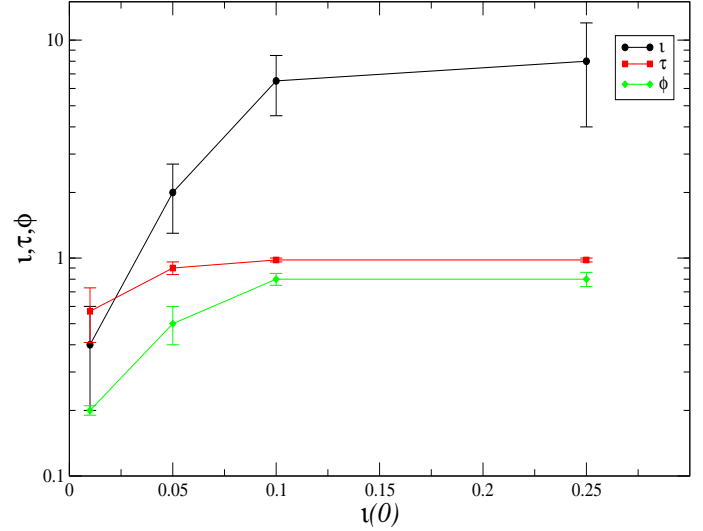


Figure 17. Upper Panel: l, τ, ϕ of ejected particles for a prolate initial ellipsoidal cloud as a function of the initial $\iota(0)$. Middle and lower panels: Projections onto two different planes of both ejected and bound particles (that are clustered in the center) for prolate initial condition with $N = 10^5$ and $\iota(0) = 0.25$. The bar-like shape of ejected particles is clearly visible.

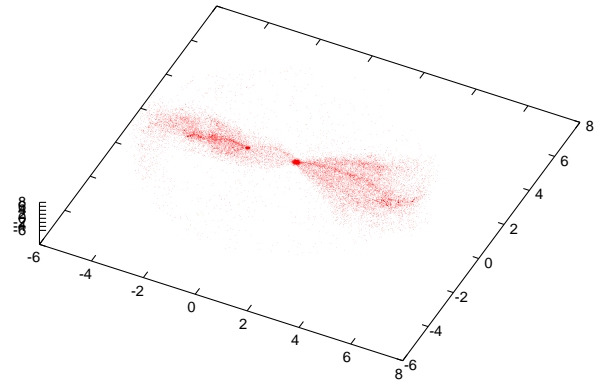
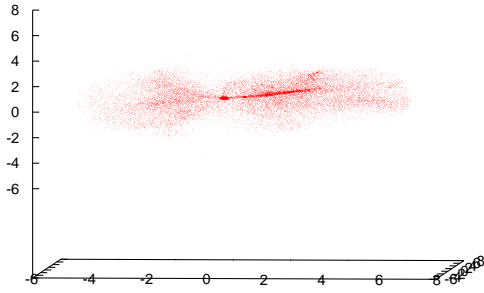
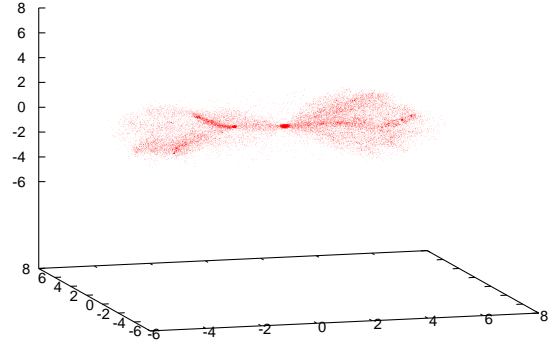
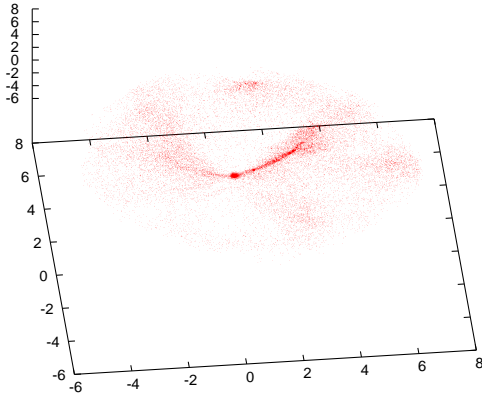
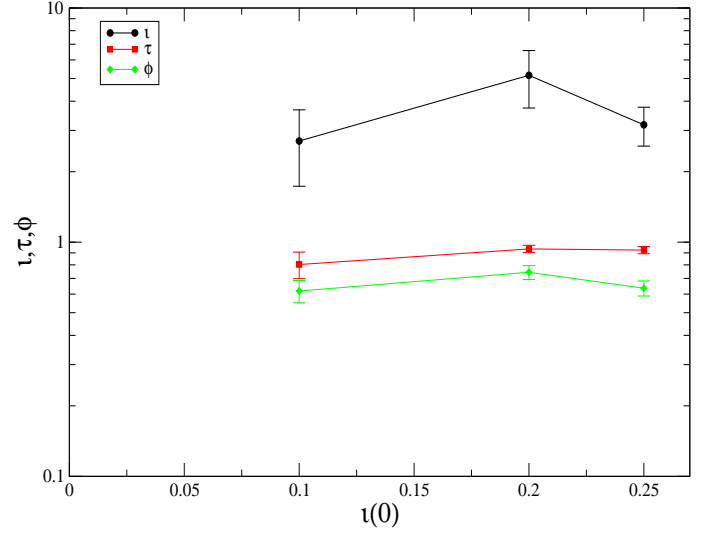
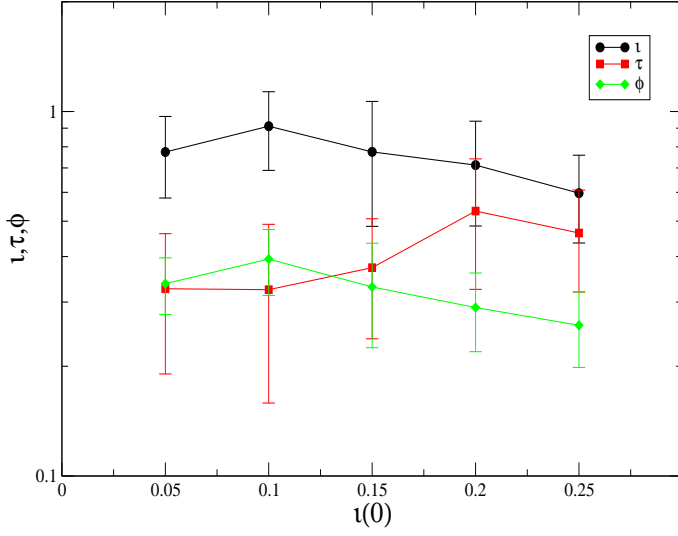


Figure 18. As Fig.17 but for oblate initial clouds with $N = 10^5$ and $\iota(0) = 0.05$.

Figure 19. As Fig.17 but for triaxial initial clouds with $N = 10^5$ with axis $a_3 = 1.1$, $a_2 = 1.05$, $a_1 = 1$.

here, i.e. a spherically symmetric stationary solutions of the collisionless Boltzmann equation with purely radial orbits. The radial orbits instability characterizing equilibrium models and systems undergoing to strong collapses and violent relaxations are distinct, but probably connected, physical mechanisms. Indeed, as firstly noticed by Merritt & Aguilar (1985) a radial instability can be the mechanism that, in the collapse of an initially cold system in which particles have mainly radial orbits, gives rise to a triaxial structure. Our findings clarify the dynamics driving the formation of a bar/disk structure in more detail than in previous works, by focusing on the relation between initial and final conditions for simple non-spherical systems. However a detailed theoretical understanding of the radial orbit instability for non-equilibrium collapsing systems is still an open problem: we refer the interested reader to a forthcoming work for a more detailed discussion about this point (Sylos Labini, Benhaïem & Joyce 2014).

On the other hand ejected particles form non-trivial anisotropic configurations, like bars or disks, that depend on the initial cloud shape: a small initial deviation from spherical symmetry is amplified by the violent relaxation energy gain mechanism and gives rise to highly non-spherical clouds. The ellipsoidal clouds that we have considered represent thus a further step toward a more realistic cloud collapse, that has allowed us to perform controlled N-body experiments to quantify the effect of the initial sphericity.

This result, although obtained for a very simplified and unrealistic physical cloud model, is interesting as it points out that it is relatively natural to generate, from an initial condition close to isotropic, a central (host) structure surrounded by particles, or even clusters of particles, that are strongly anisotropically distributed, even sometimes close to a planar distribution. Galaxy formation is a much more complex process, involving physical mechanisms such as gas dynamics, effects of dark matter halos, etc., which are not taken into account in this work. However, it is worth mentioning that recently several observational studies have pointed out that dwarf satellites of galaxies both the Milky Way and the Andromeda galaxy are non isotropically distributed around their host galaxy (see Ibata et al. (2013, 2014) and references therein). In particular it was observed that dwarf satellites are aligned in a thin plan structure and that they have coherent kinematic properties. Our results suggest that these particular features might be better understood from the collapse of a non-spherical cloud. In a forthcoming work we will consider more realistic initial conditions and a detailed comparison with observations.

We thank Michael Joyce for useful discussions and comments. We also thank an anonymous referee for a number of interesting comments that have allowed us to improve the presentation of our work. Numerical simulations have been run on the Cineca supercomputer (project ISCRA QSS-SSG) and on the super-computer Mesu of UPMC.

REFERENCES

- Aguilar, L. A. & Merritt, D. 1990, *The Astrophysical Journal*, 354, 33
- Antonov, V.A. 1961, *Soviet Astr.*, 4, 859
- Arad, I. & Johansson, P. 2005, *Monthly Notices of the Royal Astronomical Society*, 362, 252
- Barnes, E. I., Lanzel, P. A., & Williams, L. L. 2009, *The Astrophysical Journal*, 704, 372
- Bertin, G. 2000, *Dynamics of Galaxies*, by Giuseppe Bertin, pp. 430. ISBN 0521472628. Cambridge, UK: Cambridge University Press, June 2000., 1
- Binney, J. & Tremaine, S. 2011, *Galactic dynamics* (Princeton university press)
- Boily, C., Athanassoula, E., & Kroupa, P. 2002, *Monthly Notices of the Royal Astronomical Society*, 332, 971
- David, M. & Theuns, T. 1989, *Monthly Notices of the Royal Astronomical Society*, 240, 957
- Hénon, M. 1964, in *Annales d'Astrophysique*, Vol. 27, 83
- Hénon M., 1973, *Astronomy and astrophysics*, 24, 229
- Fridman & Polyachenko 1984, *Physics of Gravitating Systems I*, Chap.3, Springer-Verlag
- Ibata, N. G., Ibata, R. A., Famaey, B., & Lewis, G. F. 2014, *Nature*, 511, 563
- Ibata, R. A., Lewis, G. F., Conn, A. R., et al. 2013, *Nature*, 493, 62
- Joyce, M., Marcos, B., & Sylos Labini, F. 2009a, *Journal of Statistical Mechanics: Theory and Experiment*, 2009, P04019
- Joyce, M., Marcos, B., & Sylos Labini, F. 2009b, *Monthly Notices of the Royal Astronomical Society*, 397, 775
- Lynden-Bell, D. 1967, *Monthly Notices of the Royal Astronomical Society*, 136, 101
- Merritt D. & Aguilar L.A., 1985, *Monthly Notices of the Royal Astronomical Society*, 217, 787
- Roy, F. & Perez, J. 2004, *Monthly Notices of the Royal Astronomical Society*, 348, 62
- Springel, V. 2005, *Monthly Notices of the Royal Astronomical Society*, 364, 1105
- Springel, V., Yoshida, N., & White, S. D. 2001, *New Astronomy*, 6, 79
- Sylos Labini, F. 2012, *Monthly Notices of the Royal Astronomical Society*, 423, 1610
- Sylos Labini, F. 2013, *Monthly Notices of the Royal Astronomical Society*, 429, 679
- Sylos Labini F., Benhaïem D., Joyce M., 2015, pre-print
- Theuns, T. & David, M. 1990, *Astrophysics and Space Science*, 170, 267
- Van Albada, T. 1982, *Monthly Notices of the Royal Astronomical Society*, 201, 939
- Worrakitpoonpon, T. 2015, *Monthly Notices of the Royal Astronomical Society*, 446, 1335